



# The Mechanism of Directed Ni(II)-Catalyzed C–H Iodination with Molecular Iodine

Brandon E. Haines,<sup>a</sup> Jin-Quan Yu<sup>b</sup> and Djamaladdin G. Musaev<sup>\*,c</sup>

Received 00th January 20xx,  
Accepted 00th January 20xx

DOI: 10.1039/x0xx00000x

www.rsc.org/

Density functional theory method is used to elucidate the elementary steps of the Ni(II)-catalyzed C(sp<sup>3</sup>)–H iodination by I<sub>2</sub> with substrates bearing *N,N'*-bidentate directing centers, amide-oxazoline (AO) and 8-aminoquinoline (AQ). The relative stability of the lowest energy high- and low-spin electronic states of the catalyst and intermediates are found to be an important factor for all steps of the reaction. As a result, two-state reactivity for these systems is reported, where the reaction is initiated on the triplet surface and generates a high energy singlet nickelacycle. It is shown that the addition of Na<sub>2</sub>CO<sub>3</sub> base to the reaction mixture facilitates C–H activation. The presence of I<sub>2</sub> in the reaction provides much needed driving force for the C–H activation and nickelacycle formation, and ultimately reacts to form a new C–I bond through either a redox neutral electrophilic cleavage (EC) pathway or one-electron reductive cleavage (REC) pathway. The previously proposed Ni(II)/Ni(IV) and homolytic cleavage pathways are found to be higher in energy. The nature of substrate is found to have a large impact on the relative stability of the lowest electronic states, and on the stability of the nickelacycle resulting from C–H activation.

## Introduction

Catalytic C–H functionalization—defined as the catalytic transformation of C–H bonds into C–B, C–C, C–N, C–O, C–S and C–halogen bonds—has inherent advantages for the development of environmentally friendly and sustainable synthetic routes to complex organic targets.<sup>1–7</sup> Currently, much of the developments in this field rely on the use of expensive and rare noble metal catalysts, such as Au<sup>8–10</sup>, Pt<sup>11, 12</sup>, Pd,<sup>13, 14</sup> Rh,<sup>5, 15–18</sup> and Ir<sup>6, 18, 19</sup>. Therefore, the development of cost-effective earth-abundant transition metal catalysts (such as Fe, Co, Ni and Cu) is an attractive strategy to further capitalize on the sustainable potential of catalytic C–H functionalization.<sup>20–22</sup> However, first-row transition metals, compared with their heavier analogues, suffer from (a) more complex reactivity (i.e., more accessible oxidation states and intermediates) due to their tendency to be involved in single-electron redox processes along with two-electron redox processes,<sup>23</sup> and (b) a lack of driving force for insertion into C–H bonds because the resulting M–C and M–H bonds are weak.<sup>24</sup> Thus, innovative approaches are necessary to design earth-abundant transition metal catalysts for C–H functionalization.

Existing strategies in this field of scientific research employ photoredox<sup>25–28</sup> or chelation assisted (i.e. directing group, DG, assisted)<sup>29–47</sup> approaches. These studies have unambiguously demonstrated the effectiveness of substrates with two chelating centers, such as 8-aminoquinoline (AQ), picolinamide (PA) and others, to direct the C–H activation event.<sup>48, 49</sup> It is believed that bidentate coordination of the substrate to the metal center provides stability to the pre-reaction complex and brings the activated C–H bond in close proximity to the transition metal center.<sup>50, 51</sup> Furthermore, these studies have identified the utmost importance of controlling the multitude of oxidation states of the transition metal-centers in the course of the reaction, which may proceed via numerous pathways such as: (a) two-electron redox pathway (i.e., oxidative addition and reductive elimination), (b) single-electron oxidation/reduction pathway (for example, via reactive organic radical intermediate formation), and (c) redox neutral pathways.<sup>23</sup>

Several, recently reported, computational studies have supported above-mentioned complexity of the Ni(II)-catalyzed C–H functionalization reactions. Omer and Liu have shown that while the C(sp<sup>2</sup>)–H and C(sp<sup>3</sup>)–H bond cleavage of substrates with an 8-aminoquinoline (AQ) group by Ni(II)-catalyst occurs via the concerted metalation-deprotonation (CMD) mechanism,<sup>52, 53</sup> the mechanism of the subsequent C–C and C–X bond formation steps depends on the nature of substrate and coordination environment of metal. They may occur via either radical mechanisms (involving Ni(III) complexes) when the coupling partners are the substrates with steric-hindrance and low X–Y/X bonding energies, such as dicumyl peroxide (O–

<sup>a</sup> Cherry L. Emerson Centre for Scientific Computation, Emory University, 1515 Dickey Drive, Atlanta, Georgia 30322, E-mail: dmusaev@emory.edu

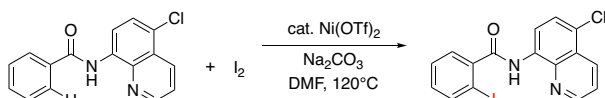
<sup>b</sup> Department of Chemistry, The Scripps Research Institute, 10550 North Torrey Pines Road, La Jolla, California 92037

<sup>†</sup> Electronic Supplementary Information (ESI) available: Additional geometrical information and free energy surfaces for the examined reaction pathways and computed energies in hartree for all reported structures. Cartesian coordinates for all reported structures are provided in xyz format. (Struct.xyz) See DOI: 10.1039/x0xx00000x

O bond), heptafluoroisopropyl iodide (3° alkyl C–I bond) and diphenyl disulfide (S–S bond), or oxidative addition/reductive elimination mechanism involving a Ni(IV) intermediate when the coupling partners are phenyl iodide (aryl C–I bond) and *n*-butyl bromide (1° alkyl C–Br bond).<sup>54</sup> Sunoj and coworkers also report that aryl iodides react through a Ni(II)/Ni(IV) manifold with C(sp<sup>3</sup>)–H AQ substrates, where the regioselectivity is determined by the reductive elimination step.<sup>55</sup> Importantly, they demonstrate that the modeling of additives in the reaction can have a large impact on the computed pathways. Thus, the nature of coupling partners (oxidants), transition metal centers and additives, as well as both nature and number of chelating centers are vital for C–H functionalization by first-row transition metal catalysts.

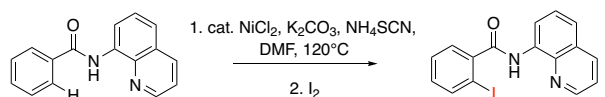
C–H iodination with molecular I<sub>2</sub> under mild experimental conditions is a highly desirable process because it utilizes inexpensive I<sub>2</sub> as the sole oxidant and increases the accessibility of synthetically valuable aryl halide compounds. The design of first-row transition metal catalysts for this reaction is expected to be even more challenging because of the ambiphilic or “chameleon” nature of the I<sub>2</sub> molecule, which can act as either an electron-donor (L-type) or electron-acceptor (Z-type) ligand in transition metal complexes.<sup>56–58</sup> As a major advancement in this field, Ni(II)-catalyzed C–H iodination with I<sub>2</sub> of an AQ substrate with *N,N'*-directing groups was recently reported by both Chatani and coworkers<sup>59</sup> and Koley and coworkers<sup>60</sup> (Figure 1). However, the mechanism of this reaction has not yet been studied in detail. Koley and coworkers proposed either Ni(II)/Ni(IV) or redox-neutral Ni(II)/Ni(II) mechanisms could be operative (Figure 2). In contrast, Chatani and coworkers settled on a Ni(II)/Ni(III) redox cycle that was previously proposed by Sanford and coworkers<sup>61, 62</sup> for C–Br bond formation from the reaction of Br<sub>2</sub> and Ni(II)(phpy)(Br)(pic), where phpy = 2-phenylpyridine and pic = 2-picoline. A notable computational study by Hall and coworkers predicted a Ni(II)/Ni(III) spin-crossover mechanism for the C–Ni bromination reaction.<sup>63</sup>

Ni: Chatani<sup>59</sup>



Also reports C(sp<sup>3</sup>)–H functionalization

Koley<sup>60</sup>



Pd: Yu<sup>64</sup>

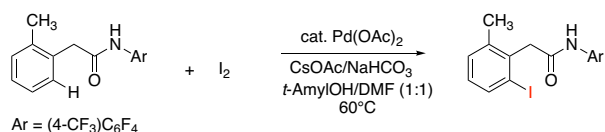


**Fig 1.** Recent representative developments in Ni(II)- and analogous Pd(II)-catalyzed C–H iodination reactions with I<sub>2</sub> as the sole oxidant.

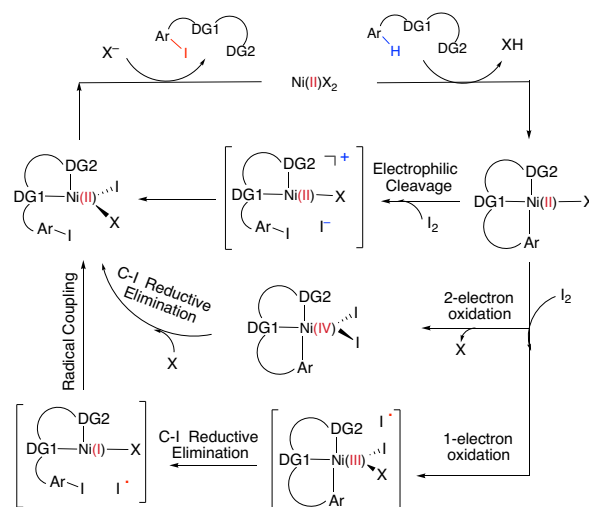


**Fig 2.** Proposed mechanisms for Ni(II)-catalyzed C–H iodination reactions with I<sub>2</sub>

To deal with the mechanistic complexity of Ni(II)-catalyzed C–H iodination with I<sub>2</sub>, the knowledge acquired for the analogous Pd(II)-catalyzed reaction<sup>64</sup> could be useful, despite known differences in the electronic structure and reactivity of the Ni(II) and Pd(II) species.<sup>65, 66</sup> In their seminal work, Yu and coworkers used commercially available monodentate acidic amide DG for the Pd(II)-catalyzed reaction,<sup>64</sup> as opposed to the *N,N'*-bidentate directing groups used for the Ni-catalyzed reaction (Figure 1). Our following extensive computational study<sup>56</sup> of this reaction revealed that C–I bond formation proceeds via a redox-neutral electrophilic cleavage (EC) mechanism initiated by coordination of I<sub>2</sub> as a Z-type ligand<sup>57, 67, 68</sup> to the axial position of the square-planar d<sup>8</sup> Ar–Pd(II) C–H activation intermediate.<sup>56</sup> Its two-electron Pd(II)/Pd(IV) oxidation mechanism, including (a) I–I oxidative addition to the Ar–Pd(II) intermediate and (b) C–I reductive elimination from the resulting Pd(IV) intermediate, is less favorable.<sup>69–71</sup> In addition, recently we have shown that the presence of a mono-*N*-protected amino acid ligand (MPAA) changes the mechanism by enabling oxidation of the Pd(II) center by I<sub>2</sub> prior to C–H activation.<sup>72</sup>

With this uncertainty surrounding the mechanism, its importance for first-row transition metal catalyst design, and the available knowledge in the literature, here we use computational methods to explore possible mechanisms and governing factors of the Ni(II)-catalyzed C–H bond iodination by molecular I<sub>2</sub> for substrates with *N,N'*-bidentate chelating groups, amide-oxazoline (AO) and AQ substrates (see Figure 3). One should note that the AO ligand, developed in Yu group, was previously used successfully for Cu-catalyzed C–H functionalization.<sup>73–77</sup> Here, we chose a common Ni(II) source, Ni(OAc)<sub>2</sub>, as a model catalyst because we aim to answer general questions about the reactivity of Ni(II) catalysts in C–H activation and iodination with I<sub>2</sub>. It is recognized that the identity of the pre-catalyst and the mechanism for entering the catalytic cycle are critical aspects of a successful reaction,

but this is not the major focus of this study. Therefore, we do not

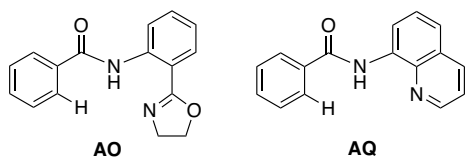


**Fig 3.** The substrates AO and AQ with *N,N'*-bidentate directing groups investigated in this paper

strive for direct correlation with all of the successful experimental reaction conditions but instead focus on general conclusions for how the catalyst achieves the critical C–H activation and iodination steps.

In general, the results of this study align with those reported by Liu<sup>54</sup> and Sunoj<sup>55</sup> but the reactivity of I<sub>2</sub> and the redox neutral EC pathway were not previously studied with computations. Furthermore, the previously reported studies<sup>50, 51, 54, 55</sup> did not fully elaborate the impact of lowest-lying electronic states of the catalyst and intermediates on the mechanism. Therefore, here, for the first time in the literature, we carefully analyze the impact of the lowest-lying singlet and triplet electronic states in Ni-catalyzed C–H functionalization. It is expected that this fundamental understanding of the Ni-catalyzed C–H iodination reactions and comparison of the acquired knowledge with that for the previously studied Pd-catalyzed reaction will enhance our ability to design cost-effective and environmentally friendly Ni-catalyzed C–H functionalization reactions and open new avenues for the design of first-row transition metal catalysts for C–H halogenation.

## Results and Discussion

### Ni(II)-catalyzed C–H Iodination of amide oxazoline (AO) substrate with I<sub>2</sub>

**Mechanism of C–H Activation.** Our extensive calculations (see Figures 4 and Supporting Information) show that the reaction of Ni(OAc)<sub>2</sub> with substrate AO is a multi-step process that proceeds via a triplet ground electronic state for the reactants, intermediates, and two concerted metalation-deprotonation (CMD) transition states (for deprotonation of N–H then C–H bonds, respectively), but leads to the singlet state nickelacycle (5-S). Thus, it is most likely that the singlet and triplet surfaces of the reaction cross, and both electronic states of the system contribute to the reactivity.

The first CMD process (i.e., deprotonation of the amide, which was not calculated) and subsequent dissociation of acetic acid completes bidentate coordination of the substrate to Ni-center with its two chelating N-groups. In the resulting (AO-*k*<sup>2</sup>-*N,N'*,*CH*)Ni(II)(OAc) complex, **3**, the *ortho*-C–H bond of the substrate phenyl group is positioned closely to the Ni-center. Subsequently, cleavage of this *ortho*-C–H bond by the second acetate ligand through CMD transition state, **TS1**, leads

to the formation of the nickelacycle (AO-*k*<sup>3</sup>-*N,N'*,*C*)Ni(II)(AcOH), **5**, with two Ni–N and one Ni–C bonds. The C–H bond deprotonation at the transition state **TS1** is found to be rate-limiting step of the process and occurs with 31.8 kcal/mol free energy barrier (on

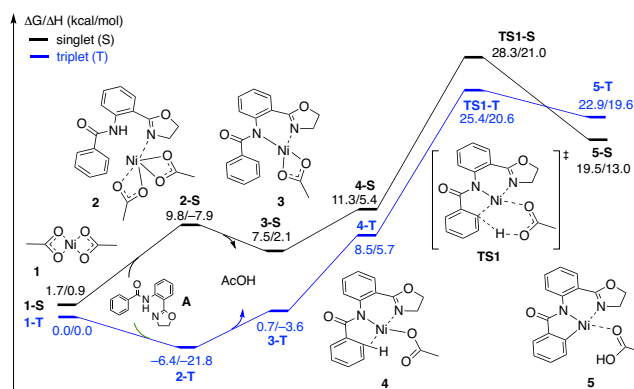


**Fig 4.** The singlet (black) and triplet (blue) free energy surfaces for AO substrate C–H bond activation starting from Ni(OAc)<sub>2</sub> catalyst. Energies are reported as  $\Delta G/\Delta H$  in kcal/mol.

the triplet state PES). Since ground electronic state of **TS1** is a triplet state, but that of nickelacycle **5** is a singlet state, it is most likely that singlet and triplet surfaces of the reaction cross *after* the triplet state C–H activation transition state. Thus, this process involves two lower-lying electronic states of the reactants, intermediates and transition states (i.e. shows two-state reactivity<sup>78</sup>). Thus, the formation of nickelacycle **5** is endergonic by 25.9 kcal/mol (Figure 4).

The computed thermodynamic instability of the nickelacycle (AO-*k*<sup>3</sup>-*N,N'*,*C*)Ni(II)(AcOH), relative to reactants Ni(OAc)<sub>2</sub> (triplet) + AO, is consistent with a previous computational study on the oxidative addition of C–H bonds to Ni(0) complexes.<sup>79</sup> This is also consistent with the deuterium labeling experiments performed by Chatani and coworkers<sup>59</sup>, the experiments of Koley and coworkers demonstrating that the nickelacycle formed by C–H activation cannot be isolated in the absence of I<sub>2</sub>,<sup>60</sup> as well as computational findings by Chen<sup>50, 51</sup> and Liu.<sup>54</sup> Additional support for this conclusion comes from the fact that nickelacycles achieved via the C–H activation are rare in the literature.<sup>80</sup> This is in contrast to analogous Pd-catalyzed reactions, where the palladacycles resulting from C–H activation thermodynamically stable and can often be isolated, characterized and used as pre-catalysts.<sup>81–83</sup> Thus, based on the above given results, we, once again, highlight one of the foremost difficulties for Ni(II)-catalyzed C–H functionalization as the lack of thermodynamic driving force for C–H activation,<sup>84</sup> which is a major reason for failure of isolation and characterization of nickelacycles from C–H activation processes. Of course, in the presence of an oxidant/electrophile, for example I<sub>2</sub>, the C–H formation barrier (i.e. reverse barrier for C–H activation) is expected to compete with either I–I bond activation (if reaction will proceed via oxidative addition mechanism), and/or C–I bond formation (if reaction proceeds via electrophilic addition mechanism),

and/or radical formation barriers. These processes are discussed in the next section.

As shown in Figure 5, the electronic state of the system has a significant impact not only on energetics but also on the geometry of the C–H activation transition states and products. (see Figure 5) The most striking difference is in the angle of the acetate base relative to the substrate coordination plane: In the triplet structures, **TS1-T** and **5-T**, the acetate is near to

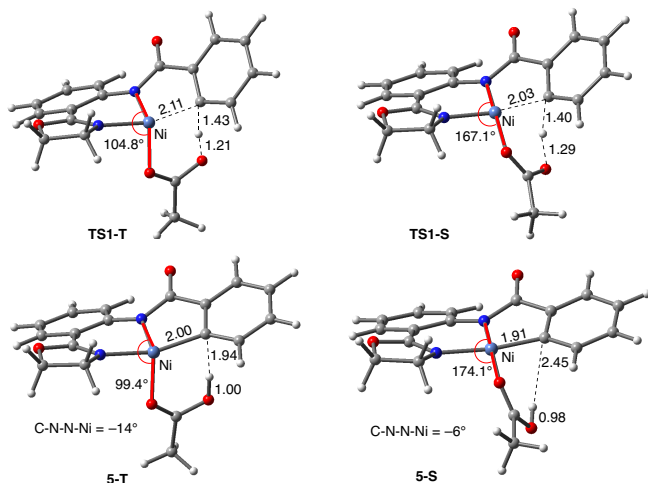


**Fig 5.** Structures of the C–H activation transition states (**TS1-T** and **TS1-S**) and products (**5-T** and **5-S**) on the triplet and singlet surfaces. Distances and angles are shown in Å and deg., respectively.

perpendicular to the substrate coordination plane (N–Ni–OAc = 104.8° and 99.4°, respectively), whereas in the singlet structures, **TS1-S** and **5-S**, the acetate is in plane with the substrate (N–Ni–OAc = 167.4° and 174.1°, respectively). It is also noted that the AO substrate is capable of twisting slightly away from planarity (in **5-T**, C–N–Ni = –14°), which may allow for some stabilization of the transition state toward the tetrahedral geometry favored on the triplet surface.<sup>63</sup>

**Role of Sodium Carbonate Additive.** Since available experiments<sup>59, 60</sup> have shown that the addition of Na<sub>2</sub>CO<sub>3</sub> base into the reaction mixture improves both reaction yield and reaction time of the Ni(II)-catalyzed C–H iodination in substrates with *N,N'*-bidentate directing groups, here, we also investigated the rate-limiting C–H activation step of this reaction in the presence of Na<sub>2</sub>CO<sub>3</sub>. In general, previous studies have indicated that the base additive may influence the C–H activation step through a) ligand exchange reactions that lead to *in situ* formation of a different catalyst,<sup>85, 86</sup> b) scavenging protons or acetic acid to drive the C–H activation,<sup>87–90</sup> and/or formation of a molecular cluster with other components (substrate, ligand, solvent, etc.) of the reaction that can promote the C–H activation step either via direct involvement in the CMD transition state or through non-covalent interactions with the substrate.<sup>91, 92</sup>

The results presented in Figure 6 show that the addition of the Na<sub>2</sub>CO<sub>3</sub> molecule to complex **3** leads to formation of the (AO-*k*<sup>2</sup>-*N,N',CH*)Ni(II)(OAc---Na<sub>2</sub>CO<sub>3</sub>), (**3-clus**) “(AcO...Na<sub>2</sub>CO<sub>3</sub>)-cluster-complex” (see ESI, Figure S1, for selected geometries):

the calculated free energy of the reaction (AO-*k*<sup>2</sup>-*N,N',CH*)Ni(II)(OAc) + Na<sub>2</sub>CO<sub>3</sub> ⇌ (AO-*k*<sup>2</sup>-*N,N',CH*)Ni(II)(OAc---Na<sub>2</sub>CO<sub>3</sub>) is –28.9 kcal/mol. This complex has a triplet ground electronic state with 1.61 |e| alpha-spin density on Ni-centers. Its open-shell singlet state (with <S<sup>2</sup>> value of 0.63) is 11.0 kcal/mol higher in free energy. From the triplet “cluster-complex” **3-clus**, the reaction may proceed either via the C–H bond activation through CMD triplet transition state **TS1-clus** by (AcO...Na<sub>2</sub>CO<sub>3</sub>) ligand, or via ligand-

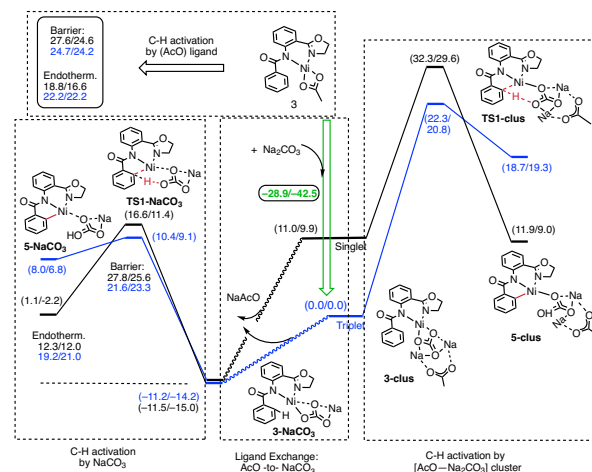


**Fig 6.** Schematic presentation of the elementary reactions involved in the addition of Na<sub>2</sub>CO<sub>3</sub> to complex (**3**). All given energies are calculated relative to triplet electronic states of the corresponding pre-reaction complexes. Energies are presented as ΔG/ΔH and in kcal/mol.

exchange (i.e. NaOAc dissociation) and subsequent C–H bond requires almost no barrier (we were not able to locate the associated transition state) and is exergonic by 11.5 kcal/mol. Thus, one may confidently conclude that the addition of Na<sub>2</sub>CO<sub>3</sub> molecule to the reaction mixture will produce AcO-to-NaCO<sub>3</sub> ligand exchange and will generate the new catalytic active species (AO-*k*<sup>2</sup>-*N,N',CH*)Ni(II)(NaCO<sub>3</sub>). In this newly generated active species, the C–H bond activation requires 21.6 kcal/mol free energy barrier and is endergonic by 12.3 kcal/mol. Comparison of these energy parameters for active species (AO-*k*<sup>2</sup>-*N,N',CH*)Ni(II)(NaCO<sub>3</sub>) with those, 24.7 kcal/mol free energy barrier and 18.8 kcal/mol endergonicity, for (AO-*k*<sup>2</sup>-*N,N',CH*)Ni(II)(OAc) (calculated relative to **3-T**) clearly demonstrates the benefits of the presence of Na<sub>2</sub>CO<sub>3</sub> in the reaction conditions. This is consistent with the findings of Liu and coworkers that a Ni(NaCO<sub>3</sub>)<sub>2</sub>•4DMF catalyst is the likely active catalyst in their systems).<sup>54</sup> To summarize, the addition of Na<sub>2</sub>CO<sub>3</sub> to the reaction mixture (a) generates new catalytic active species (AO-*k*<sup>2</sup>-*N,N',CH*)Ni(II)(NaCO<sub>3</sub>) with small or no energy barrier, (b) reduces rate-limiting C–H activation barrier by 3.1 kcal/mol, and (c) stabilizes the C–H activation product by 6.3 kcal/mol.

**Mechanism of Iodination with I<sub>2</sub>** The next step of the reaction of substrate AO with I<sub>2</sub> is addition of oxidant to nickelacycle **5-S**. This process is found to be thermodynamically favorable, provides an additional stabilization to the C–H activation



product and, consequently, increases the barrier of the reverse reaction (i.e., C–H bond formation). A similar result was previously reported for  $I_2$  addition to a palladacycle in our study on the analogous Pd(II)-catalyzed reaction.<sup>56</sup> Coordination of  $I_2$  to the axial position of nickelacycle **5-S** to form **6-S** is exergonic by 9.4 kcal/mol. However, it is still endergonic by 10.1 kcal/mol relative to the dissociation limit of **1-T** + AO +  $I_2$ . The geometric signatures of the resulting complex **6-S** — elongation of the I–I bond from 2.87 Å in free  $I_2$  to 3.11 Å in **6-S** and linearity of the interaction between Ni and  $I_2$  (with  $\angle Ni-I-I = 167.2^\circ$ ) — imply

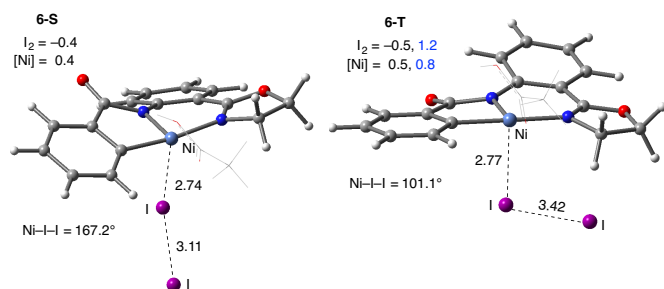


**Fig 7.** Structural features of the  $I_2$  coordination complexes (**6-S**) and (**6-T**). Distances are in Å, angles are in degrees and fragment Mulliken charge and spin density (in  $|e|$ ) are shown as black and blue, respectively. For simplicity of presentation, the AcOH ligand is shown in wireframe representation.

donation of partial electron from the Ni  $d_{22}$  orbital into the  $I_2$   $\sigma^*$  orbital<sup>56, 58</sup> (See Figure 7).

Consistently, the triplet electronic state of the  $I_2$  coordination complex (**6-T**) becomes only 0.7 kcal/mol higher in free energy than its singlet state counterpart **6-S**. Analysis of unpaired spin densities (with 1.2  $|e|$  and 0.8  $|e|$ , on the  $I_2$  and Ni fragments, respectively) allows us to characterize **6-T** as a Ni(III)– $I_2$  complex formed by one electron transfer from Ni-center to  $I_2$  (the calculated Mulliken charges of the  $I_2$  and Ni fragments are  $-0.5 |e|$  and  $0.5 |e|$ , respectively).<sup>63</sup> (Figure 7) As a result of this full (rather than partial) Ni-to- $I_2$  electron transfer, the elongation of the I–I bond (3.42 Å) becomes more pronounced than in **6-S** and the  $\angle Ni-I-I$  angle becomes bent ( $101.1^\circ$ ).

The accessibility of the triplet state complex **6-T** upon single electron transfer from Ni to  $I_2$  makes the reactivity of the nickelacycle with  $I_2$  more complex than that of its Pd analogue. Indeed, as illustrated in Figure 8, one can expect two distinct iodination pathways for each of the singlet and triplet state complexes **6-S** and **6-T**. For the singlet **6-S** complex, the pathways are analogous to those studied for the Pd-catalyzed reaction: (A) a redox neutral Ni(II)/Ni(II) pathway proceeding through concerted electrophilic cleavage (EC) of  $I_2$  and concomitant C–I bond formation (black solid line in Figure 8); and (B) a Ni(III)/Ni(IV) pathway proceeding through I–I oxidative addition (OA) followed by C–I reductive elimination (black dashed line in Figure 8). For the triplet state **6-T** complex, these pathways are (C) a single electron reductive electrophilic cleavage (REC) Ni(III)/Ni(II) process in which C–I bond formation and one electron reduction of the Ni(III) center

occur simultaneously (blue solid line in Figure 8), and (D) a radical mechanism (RA) in which cleavage of the I–I bond forms a Ni(III) complex and iodine atom (blue dashed line in Figure 8). It is possible that these pathways can interconvert to each other by crossing between the singlet and triplet surfaces. Below, we discuss these processes in more details. (For sake of simplicity, the free energies discussed in this section are calculated relative to the singlet state complex **6-S**).

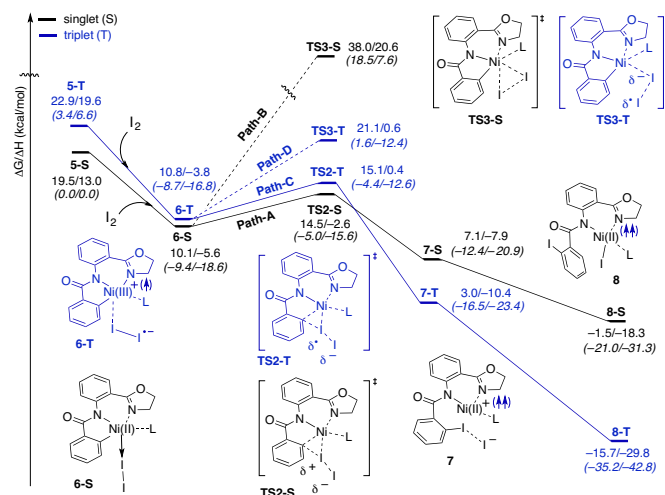


**Fig 8.** The singlet (black) and triplet (blue) free energy surfaces for AO substrate C–H bond iodination. Energies are reported as DG/DH in kcal/mol. Numbers given in first and second lines are relative to dissociation limits of Ni(AcO)<sub>2</sub> (triplet) + AO +  $I_2$  and **5-S** +  $I_2$ , respectively. Here, L stands for AcOH.

**Path-A: Redox neutral Ni(II)/Ni(II) electrophilic cleavage (EC) mechanism.** This pathway of the reaction is initiated by electrophilic attack of  $I_2$  on the Ni(II)–C bond at the transition state (**TS2-S**). As shown in Figure 9, at **TS2-S** the proximal iodonium engages in bonding with the Ni and C centers (with Ni–I = 2.95 Å and I–C = 2.47 Å) while the terminal iodide is displaced (with I–I = 3.26 Å). The free energy barrier associated with this transition state is only 4.4 kcal/mol, which is much smaller than overall 16.0 kcal/mol barrier required for the reverse C–H activation (i.e., C–H bond formation). (see Figures 4 and 8) Thus, addition of  $I_2$  to reaction mixture of Ni(OAc)<sub>2</sub> and AO substrate makes C–H activation and, consequently, C–H iodination irreversible. IRC calculations initiated from the transition state (**TS2-S**) show that in the EC product (**7-S**) the C–I bond is formed and the expelled iodide forms an ion-pair with a Ni(II)<sup>+</sup> center. Formation of **7-S** is exergonic by 3.0 kcal/mol, and combination of the Ni(II)<sup>+</sup> and iodide ions to produce the Ni(II)–I intermediate **8-S** is exergonic by 8.6 kcal/mol.

**Path-B: Ni(II)/Ni(IV) 2-electron oxidation pathway.** This pathway starts by oxidative insertion of Ni(II) into the I–I bond at the transition state **TS3-S**, where the breaking I–I bond is I–I = 3.27 Å, but forming  $I_{eq}$ –Ni and  $I_{ax}$ –Ni bonds are 2.99 and 3.19

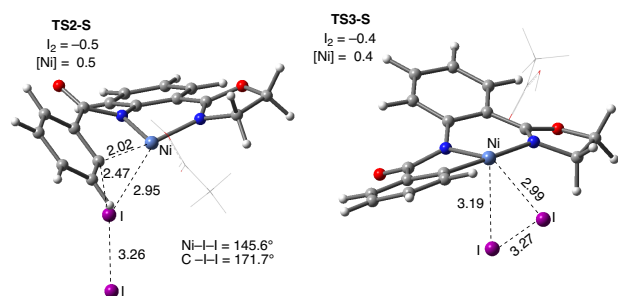


**Fig 9.** Structural features of iodination transition states on the singlet surface, electrophilic cleavage (**TS2-S**) and oxidative addition (**TS3-S**). Distances are in Å, angles are in degrees and fragment Mulliken charges are in |e|. For simplicity of presentation, the AcOH ligand is shown in wireframe representation.

Å, respectively (see Figure 9). The free energy barrier associated with this oxidative addition transition state is 27.9 kcal/mol, which is 23.5 kcal/mol higher than that required for electrophilic cleavage (EC) pathway (Path-A) (see Figure 8). These conclusions for the EC and OA pathways are consistent with our previous study on Pd-catalyzed C–H iodination where the redox neutral, Pd(II)/Pd(II) pathway is also shown to be more favorable than Pd(II)/Pd(IV) mechanism.<sup>56</sup> Since the OA pathway cannot compete with EC pathway, here we will not discuss this OA pathway in more detail, while we include full computational data on the OA pathway in the ESI (see Figure S2). We also investigated the possibility of dissociation of L, AcOH in this case, from **6-S** to facilitate oxidative addition. We found this process to have a slightly lower overall barrier (**6-S** → **TS3-S-I2**,  $\Delta G^\ddagger = 25.2$  kcal/mol) than the reaction through **TS3-S**. (See ESI for more details.) Regardless, this reaction pathway is much higher than the EC pathway.

**Path-C: Ni(II)/Ni(III) single electron reductive electrophilic cleavage (REC).** The one-electron oxidation process of converting **6-S** to **6-T** (i.e. Ni(III)<sup>+</sup>–I<sub>2</sub><sup>–</sup> complex) initiates this pathway. In the next step, the Ni(III)<sup>+</sup>–C bond abstracts an iodine atom from I<sub>2</sub><sup>–</sup>, which reduces the Ni(III) center and releases iodide. Thus, this pathway couples one-electron reduction of the metal with electrophilic cleavage (REC). Mulliken charge and spin density analysis of the I<sub>2</sub> (–0.4 |e| and 0.7 |e|) and Ni (0.4 |e| and 1.3 |e|) fragments of the associated transition state (**TS2-T**) shows spin density transfer from I<sub>2</sub><sup>–</sup> to Ni complex. (Figure 10) Of particular interest, the distal I has significant negative charge (–0.5 |e|) while the proximal I does not (0.1 |e|). Overall, the geometry of **TS2-T** is similar to **TS2-S** except that the Ni center and I<sub>2</sub><sup>–</sup> have a bent geometry (Ni–I–I = 117.0°) and the proximal iodine atom interacts more closely with the Ni center (I–Ni = 2.47 Å). Like in **TS2-S**, the terminal iodide is displaced (I–I = 3.31 Å) while the new I–C bond is forming (I–C = 2.72 Å). The free energy barrier (calculated relative to complex **6-S**) for the REC pathway is found to be 5.0 kcal/mol, which is 0.6 kcal/mol higher than the EC pathway on the singlet surface. The product complex, **7-T**, is an ion-pair between Ni(III)<sup>+</sup> and iodide analogous of **7-S** except that the Ni(II) is high-spin (spin density of 1.62 |e| on the Ni center). Formation of **7-T** is exergonic by 7.1 kcal/mol, and combination of the Ni(III)<sup>+</sup> and iodide ions to produce **8-T** is exergonic by 18.7 kcal/mol.

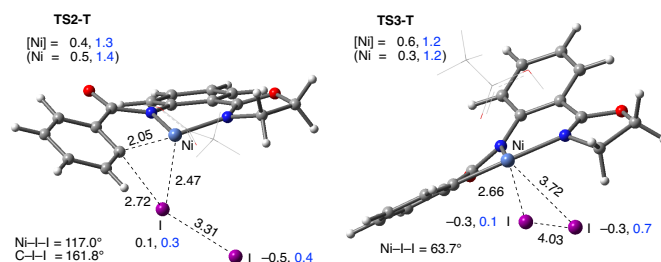


**Fig 10.** Structural features of iodination transition states on the triplet surface, REC (**TS2-T**) and RA (**TS3-T**). Distances are in Å, angles are in degrees and fragment Mulliken charge and spin density (in |e|) are shown as black and blue, respectively. For simplicity of presentation, the AcOH ligand is shown in wireframe representation.

With the expulsion of I<sup>–</sup> during the reaction, we also investigated the role of I<sub>3</sub><sup>–</sup> complex formation in the presence of excess I<sub>2</sub>. We compute I<sub>3</sub><sup>–</sup> formation from I<sub>2</sub> and I<sup>–</sup> to be exergonic by 12.3 kcal/mol. This suggests that I<sub>3</sub><sup>–</sup> complex formation could be playing the role of providing additional driving force for I<sup>–</sup> generation. Indeed, coordination of an additional molecule of I<sub>2</sub> to complexes **7-S** and **7-T** to form **7-S-I3** and **7-T-I3**, respectively are exergonic by 15.6 and 13.0 kcal/mol, respectively. Thus, we propose that the EC and REC pathways can be facilitated by I<sub>3</sub><sup>–</sup> formation.

**Path-D: Ni(II)/Ni(III) single electron radical pathway (homolytic cleavage).** This pathway is also initiated by Ni(III)<sup>+</sup>–I<sub>2</sub><sup>–</sup> intermediate, **6-T**. In the next step, the I–I bond of I<sub>2</sub><sup>–</sup> is cleaved through iodide abstraction by the cationic Ni(III) center (i.e., charge recombination) to produce a Ni(III)–I intermediate and iodine atom. Here we refer to this pathway as the radical pathway (RA), but it is analogous to the homolytic cleavage pathway described by Liu.<sup>54</sup> In the associated transition state (**TS3-T**), Mulliken spin density analysis of the I<sub>2</sub> fragment shows that the distal I has significant radical character (0.7 |e|) while the proximal I has little (0.1 |e|) (Figure 10). In the TS, the bond between the proximal iodine atom and the Ni center is almost fully formed (I–Ni = 2.66 Å) and the distal iodine atom does not form any strong interactions. (I–I = 4.03 Å, Ni–I = 3.72 Å). The free energy barrier (calculated relative to complex **6-S**) for the RA pathway is 11.0 kcal/mol, which is 6.6 kcal/mol higher than the EC pathway and 6.0 kcal/mol higher than the REC pathway. The RA pathway will not compete with the EC and REC pathways, so we will not discuss it in more detail, but we include its full computational data in the ESI (see Figure S2).

**Catalytic Cycle.** Extensive analysis of these reaction pathways shows that they converge to common Ni(II)–I intermediates **8-S** on the singlet surface and **8-T** on the triplet surface (Figure 8). The high spin Ni(II)–I intermediate **8-T** is lower in free energy than its singlet analogue **8-S** by 14.2 kcal/mol indicating that the overall C–H iodination reaction has a much larger driving force on the triplet surface than on the singlet surface. From **8-T**, catalytic cycle is closed by i) reprotonation of the substrate amide by acetic acid (i.e., (AO-*k*<sup>3</sup>-N,N',C)Ni(II)(AcOH)(I) → (AO-*k*<sup>3</sup>-N,NH',C)Ni(II)(OAc)(I)), and ii)

displacement of iodide and the iodinated product (AO-I) by acetates to regenerate the  $\text{Ni}(\text{OAc})_2$  catalyst. If we also invoke the role of the strong base,  $\text{Na}_2\text{CO}_3$ , to remove the C-H proton from solution, then the overall reaction,  $\text{Ni}(\text{OAc})_2$  (**1-T**) + AO +  $\text{I}_2$  +  $\text{Na}_2\text{CO}_3 \rightarrow \text{Ni}(\text{OAc})_2$  (**1-T**) + AO-I + NaI +  $\text{NaHCO}_3$ , becomes exergonic by 20.8 kcal/mol.

In summary, the consideration of several reaction pathways for Ni-C bond iodination with  $\text{I}_2$  reveals that the redox neutral Ni(II)/Ni(II) electrophilic cleavage (EC) and Ni(II)/Ni(III) single electron reductive electrophilic cleavage (REC) pathways are the most likely mechanisms for this reaction. The computed barrier for the EC pathway is the lowest for the AO substrate, but the computed barrier for the REC pathway is only 0.6 kcal/mol higher. The previously studied 2-electron Ni(II)/Ni(IV) oxidative addition/reductive elimination (OA) and Ni(II)/Ni(III)

(calculated relative to the triplet complex **AQ-2-T**) at the transition state **AQ-TS1-S**, which is *ca.* 2 kcal/mol larger than that reported for the substrate AO (Figure 4). In contrast to substrate AO, the rate-limiting C-H activation transition state for substrate AQ, **AQ-TS1-S**, has a singlet ground electronic state: its triplet state counterpart **AQ-TS1-T** lies by 2.3 kcal/mol higher. Thus, the singlet-triplet surface crossing likely occurs *before* the rate-limiting C-H activation transition state for substrate AQ. Indeed, we were able to locate a minimum energy crossing point (**AQ-mecp**) that is close in energy (13.0 kcal/mol) and geometry to the singlet reactant structure **AQ-4-S**. (Figures 11 and 12) The nature of substrate also has a significant impact on the stability of the nickelacycles resulting from the C-H activation. As mentioned above, for substrate AO, overall process  $\text{Ni}(\text{OAc})_2$  (triplet) + AO  $\rightarrow$  **5-S** is endergonic by 19.5 kcal/mol. In contrast,

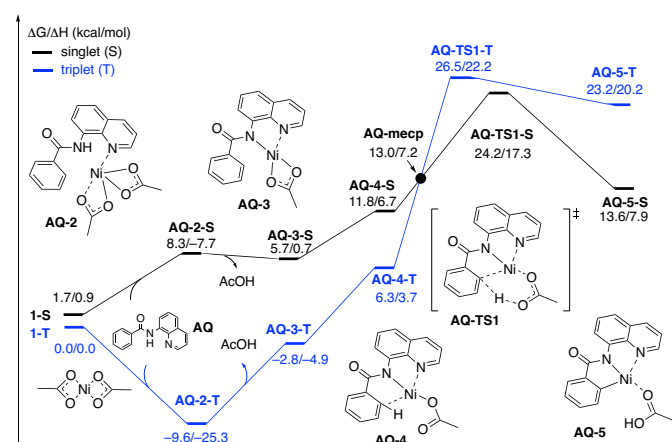


**Fig 11.** The singlet (black) and triplet (blue) free energy surfaces for C-H bond activation in AQ substrate by  $\text{Ni}(\text{OAc})_2$  catalyst. Energies are reported as DG/DH in kcal/mol.

radical (RA, homolytic cleavage) pathways are found to be higher in energy for  $\text{I}_2$ . Given that the reactivity is highly dependent on the identity of the oxidant/electrophile, these results suggest that the EC and REC pathways should also be considered for Ni-catalyzed C-H functionalization reactions.

### Ni(II)-catalyzed C-H Iodination of 8-aminoquinoline (AQ) substrate with $\text{I}_2$

To provide further validation and connection to experiments, we also studied Ni(II)-catalyzed C-H bond iodination with  $\text{I}_2$  of substrate AQ. We believe that our calculated results are going to be helpful in understanding and rationalizing experimental findings by Chatani<sup>59</sup> and Koley<sup>60</sup>, as well as in predicting of novel ligands. In general, we find that substrate AQ gives qualitatively the same results as substrate AO with a few interesting differences that will be discussed here briefly. The full details of the calculations with substrate AQ can be found in the ESI (See Figure S3).

Firstly, as shown in the calculated potential energy surface in Figure 11, the C-H activation of substrate AQ by  $\text{Ni}(\text{OAc})_2$  requires an overall 33.8 kcal/mol free energy barrier

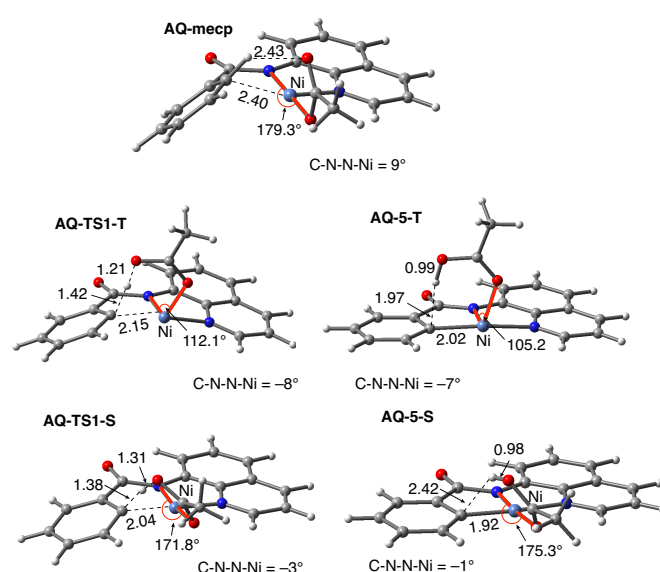


**Fig 12.** Structural features of the C-H activation transition states with substrate AQ (**AQ-TS1-T** and **AQ-TS1-S**) and products (**AQ-5-T** and **AQ-5-S**) on the triplet and singlet surfaces. Distances are shown in Å and angles are shown in deg.

this process for substrate AQ, i.e. reaction  $\text{Ni}(\text{OAc})_2$  (triplet) + AQ  $\rightarrow$  **AQ-5-S**, is endergonic only by 13.6 kcal/mol.

Thus, the replacement of substrate AO by substrate AQ a) shifts the C-H bond activation reaction to the singlet surface and triplet-to-singlet surface crossing occurs before the C-H activation transition state, b) makes the overall process thermodynamically more favorable by 5.9 kcal/mol, and (c) only slightly (*ca.* 2 kcal/mol) increases rate-limiting C-H activation barrier. Thermodynamic preference of the C-H activation in AQ compared by AO can be explained by careful analysis of the geometries of the corresponding final products. Indeed, nickelacycle **AQ-5-S** has a square planar geometry with  $\angle(\text{Ni}-\text{N}-\text{N}-\text{C})$  angle of  $-1^\circ$  through the formation of a fused [3.3.0] ring system (Figure 12), whereas the nickelacycle of **5-S** is more twisted out of plane ( $\text{Ni}-\text{N}-\text{N}-\text{C} = -6^\circ$ ) because of additional ring strain introduced by the larger [4.3.0] fused ring system.

(Figure 6) This analysis is consistent with the findings of Chen and coworkers.<sup>50, 51</sup>

Secondly, in contrast to substrate AO, for substrate AQ, the triplet  $I_2$ -coordination complex **AQ-6-T**, which lies 4.7 kcal/mol higher than reactants **AQ-1-T** +  $I_2$ , is slightly (by 0.5 kcal/mol) lower than its singlet counterpart **AQ-6-S**. (See ESI, Figure S3) Likewise, Ni(II)/Ni(III) single electron reductive electrophilic cleavage (REC) free energy barrier (Path-C, initiated from the **AQ-6-T** complex) at the transition state **AQ-TS2-T** is calculated to be lower than the redox neutral Ni(II)/Ni(II) electrophilic cleavage (EC) free energy barrier (Path-A, initiated from the **AQ-6-S** complex and following via the transition state **AQ-TS2-S**). Based on these results, it appears that the C–H iodination reaction in substrate AQ will revert back to the triplet surface much earlier on the reaction coordinate (i.e. during  $I_2$  coordination) than that was the case with substrate AO. However, like substrate AO, the Ni(II)/Ni(III) single electron reductive electrophilic cleavage (REC) and redox neutral Ni(II)/Ni(II) electrophilic cleavage (EC) pathways remain close in

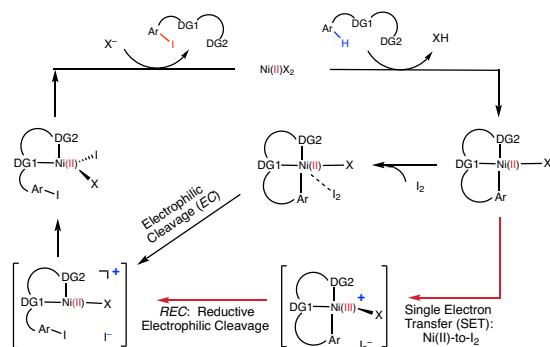


**Fig 13.** Mechanism proposed for Ni-catalyzed C–H iodination with  $I_2$  based on DFT calculations in this study.

energy for substrate AQ. This suggests that modulation of the substrate structure (or reaction conditions) can switch between them and still achieve C–I bond formation. Significantly, these data clearly demonstrate the importance of the availability of the lowest-lying electronic states of the first-row transition metal centers for C–H iodination in substrates with an  $N,N'$ -bidentate chelating groups: The actual mechanism of the reaction directly relates to stability and energy difference between lowest high- and low-spin electronic states.

## Conclusions

Extensive calculations on the elementary steps of Ni(II)-catalyzed C–H iodination by  $I_2$  with two substrates with  $N,N'$ -bidentate directing groups (AO and AQ) have revealed the most likely reaction mechanism as illustrated in Figure 13. Importantly, we found the relative stability of the lowest energy high- and low-spin electronic states to be an important factor for all steps of the reaction. We expect this to be a general feature of first-row transition metal catalysts in C–H functionalization. We found that:

1. The reaction is initiated by substrate coordination to the triplet  $Ni(OAc)_2$  complex and N–H deprotonation to form a stable triplet ( $SUB-k^2-N,N',CH$ )Ni(II)(OAc) complex. Calculated stabilization energy is 6.4 and 9.6 kcal/mol for substrates AO and AQ, respectively.
2. From ( $SUB-k^2-N,N',CH$ )Ni(II)(OAc), C–H activation occurs via the base-assisted CMD mechanism on either the triplet surface (for substrate AO) or the singlet surface (for substrate AQ) and generates singlet Ni(II)-nickelacycles. This process requires significant free energy barrier (31.8 kcal/mol for AO and 33.8 kcal/mol for AQ), occurs via triplet-to-singlet spin crossover and is endergonic by 19.5 kcal/mol for AO and 13.6 kcal/mol for AQ. Thus, in the absence of oxidant (or coupling partners) this C–H activation process is not feasible, which is consistent with experiments.<sup>60</sup>
3. However, in the presence of  $I_2$  as an oxidant, the coordination of  $I_2$  to Ni(II)-nickelacycle provides additional stability to the C–H activation product. In both the singlet and triplet states of the resulting nickelacycle- $I_2$  complex **6**,  $I_2$  accepts electron density from the Ni complex. Since in the triplet state nickelacycle- $I_2$  complex **6-T** almost one electron is transferred to  $I_2$ , it was characterized as a  $[Ni(III)^+ \cdots I_2^-]$  ion-paired complex.
4. The subsequent C–I bond formation is very fast through either the redox-neutral EC pathway, if reaction starts from the singlet **6-S** complex, or one-electron REC pathway, if reaction starts from the triplet **6-T** complex. Both pathways lead to the formation of a stable, high spin Ni(II)–I intermediate.
5. The addition of base  $Na_2CO_3$  to the reaction mixture initiates  $AcO$ -to- $NaCO_3$  ligand exchange and generates the ( $SUB-k^2-N,N',CH$ )Ni(II)( $NaCO_3$ ) active catalyst. This ligand exchange reaction is exergonic for substrate AO and requires insignificant energy barrier. Furthermore, involvement of new base, i.e.  $Na_2CO_3$ , reduces rate-limiting C–H activation barrier by 3.1 kcal/mol and stabilizes the C–H activation product by 6.3 kcal/mol. These findings are consistent with experiments showing that  $Na_2CO_3$  helps facilitate Ni-catalyzed C–H iodination with  $I_2$ .<sup>59, 60</sup>
6. Replacement of substrate AO by substrate AQ affects the energy difference between the lowest high- and low-spin electronic states of the systems in several places along the reaction pathway. It makes the C–H activation step thermodynamically more favorable by 5.9 kcal/mol, and only slightly (*ca.* 2 kcal/mol) increases rate-limiting C–H activation barrier. Thus, computations indicate that the substrate AO is also viable for Ni(II)-catalyzed C–H iodination with  $I_2$ .

## Computational Details

Calculations were performed with the Gaussian 09 (G09) program.<sup>93</sup> Geometry optimizations and frequency calculations for all reported structures were performed at the B3LYP-D3/[6-31G(d,p) + Lanl2dz (Pd, I)] level of theory with the



corresponding Hay-Wadt corresponding effective core potential for Pd and I,<sup>94-96</sup> and Grimme's empirical dispersion-correction (D3) for B3LYP.<sup>97</sup> Each reported minimum has zero imaginary frequencies and each transition state (TS) structure has only one imaginary frequency. Intrinsic reaction coordinate (IRC) calculations were performed for selected transition state structures to confirm their identity. Bulk solvent effects are incorporated for all calculations using the self-consistent reaction field polarizable continuum model (IEF-PCM)<sup>98-100</sup> with dimethylsulfoxide (DMSO) as the solvent. The calculated Gibbs free energies are corrected to a solution standard state of 1M at room temperature (298.15K).<sup>101, 102</sup>

It is known that Ni-complexes may have several energetically close lower-lying electronic states,<sup>63</sup> therefore, herein we investigate both the ground and first excited states of reactants, intermediates, transition states and products of the reaction. Some structures on the singlet potential energy surface have lower energy open-shell singlet electronic states. In these cases, we re-calculated the geometries and energies of the structures at their open-shell singlet electronic states using unrestricted DFT (UB3LYP-D3).<sup>103, 104</sup> Minimum energy crossing points (MECP) between singlet and triplet states were located using the MECPro program (v. 1.0.3) developed by Ess and coworkers<sup>105</sup> with G09.

## Conflicts of interest

There are no conflicts to declare.

## Acknowledgements

This work was supported by the National Science Foundation under the CCI Center for Selective C–H Functionalization (CHE-1700982). We gratefully acknowledge NSF MRI-R2 grant (CHE-0958205 for D.G.M.) and the use of the resources of the Cherry Emerson Center for Scientific Computation. We also thank Dr. R. Roszak for helpful discussions, and Prof. D. H. Ess (BYU) for providing access to his MECPro code (v. 1.0.3).

## Notes and references

- 1 L. Ackermann, *Chem. Rev.*, 2011, **111**, 1315-1345.
- 2 T. Bruckl, R. D. Baxter, Y. Ishihara and P. S. Baran, *Acc. Chem. Res.*, 2012, **45**, 826-839.
- 3 K. M. Engle, T. S. Mei, M. Wasa and J. Q. Yu, *Acc. Chem. Res.*, 2012, **45**, 788-802.
- 4 K. Godula and D. Sames, *Science*, 2006, **312**, 67-72.
- 5 H. M. L. Davies and J. R. Manning, *Nature*, 2008, **451**, 417-424.
- 6 J. F. Hartwig, *J. Am. Chem. Soc.*, 2016, **138**, 2-24.
- 7 C. J. Li and B. M. Trost, *Proc. Natl. Acad. Sci. U.S.A.*, 2008, **105**, 13197-13202.
- 8 A. Arcadi, *Chem. Rev.*, 2008, **108**, 3266-3325.
- 9 T. de Haro and C. Nevado, *Synthesis (Stuttg.)*, 2011, DOI: 10.1055/s-0030-1260122, 2530-2539.
- 10 J. Xie, C. D. Pan, A. Abdukader and C. J. Zhu, *Chem. Soc. Rev.*, 2014, **43**, 5245-5256.
- 11 M. Lersch and M. Tilset, *Chem. Rev.*, 2005, **105**, 2471-2526.
- 12 S. S. Stahl, J. A. Labinger and J. E. Bercaw, *Angew. Chem., Int. Ed.*, 1998, **37**, 2181-2192.
- 13 X. Chen, K. M. Engle, D. H. Wang and J. Q. Yu, *Angew. Chem., Int. Ed.*, 2009, **48**, 5094-5115.
- 14 T. W. Lyons and M. S. Sanford, *Chem. Rev.*, 2010, **110**, 1147-1169.
- 15 D. A. Colby, R. G. Bergman and J. A. Ellman, *Chem. Rev.*, 2010, **110**, 624-655.
- 16 D. A. Colby, A. S. Tsai, R. G. Bergman and J. A. Ellman, *Acc. Chem. Res.*, 2012, **45**, 814-825.
- 17 M. P. Doyle, R. Duffy, M. Ratnikov and L. Zhou, *Chem. Rev.*, 2010, **110**, 704-724.
- 18 K. Shin, H. Kim and S. Chang, *Acc. Chem. Res.*, 2015, **48**, 1040-1052.
- 19 I. A. I. Mkhalid, J. H. Barnard, T. B. Marder, J. M. Murphy and J. F. Hartwig, *Chem. Rev.*, 2010, **110**, 890-931.
- 20 H. M. L. Davies and D. Morton, *J. Org. Chem.*, 2016, **81**, 343-350.
- 21 A. A. Kulkarni and O. Daugulis, *Synthesis (Stuttg.)*, 2009, **24**, 4087-4109.
- 22 B. Su, Z. C. Cao and Z. J. Shi, *Acc. Chem. Res.*, 2015, **48**, 886-896.
- 23 S. Z. Tasker, E. A. Standley and T. F. Jamison, *Nature*, 2014, **509**, 299-309.
- 24 J. Uddin, C. M. Morales, J. H. Maynard and C. R. Landis, *Organometallics*, 2006, **25**, 5566-5581.
- 25 D. R. Heitz, J. C. Tellis and G. A. Molander, *J. Am. Chem. Soc.*, 2016, **138**, 12715-12718.
- 26 M. H. Shaw, V. W. Shurtleff, J. A. Terrett, J. D. Cuthbertson and D. W. C. MacMillan, *Science*, 2016, **352**, 1304-1308.
- 27 B. J. Shields and A. G. Doyle, *J. Am. Chem. Soc.*, 2016, **138**, 12719-12722.
- 28 Z. W. Zuo, D. T. Ahneman, L. L. Chu, J. A. Terrett, A. G. Doyle and D. W. C. MacMillan, *Science*, 2014, **345**, 437-440.
- 29 L. C. M. Castro and N. Chatani, *Chem. Lett.*, 2015, **44**, 410-421.
- 30 Y. Aihara and N. Chatani, *J. Am. Chem. Soc.*, 2013, **135**, 5308-5311.
- 31 Y. Aihara and N. Chatani, *J. Am. Chem. Soc.*, 2014, **136**, 898-901.
- 32 X. F. Cong, Y. X. Li, Y. Wei and X. M. Zeng, *Org. Lett.*, 2014, **16**, 3926-3929.
- 33 M. L. Li, J. X. Dong, X. L. Huang, K. Z. Li, Q. Wu, F. J. Song and J. S. You, *Chem. Commun.*, 2014, **50**, 3944-3946.
- 34 H. Shiota, Y. Ano, Y. Aihara, Y. Fukumoto and N. Chatani, *J. Am. Chem. Soc.*, 2011, **133**, 14952-14955.
- 35 W. F. Song, S. Lackner and L. Ackermann, *Angew. Chem., Int. Ed.*, 2014, **53**, 2477-2480.
- 36 X. S. Wu, Y. Zhao and H. B. Ge, *J. Am. Chem. Soc.*, 2014, **136**, 1789-1792.
- 37 X. S. Wu, Y. Zhao and H. B. Ge, *Chem. Eur. J.*, 2014, **20**, 9530-9533.
- 38 Y. Aihara, M. Tobisu, Y. Fukumoto and N. Chatani, *J. Am. Chem. Soc.*, 2014, **136**, 15509-15512.
- 39 M. Iyanaga, Y. Aihara and N. Chatani, *J. Org. Chem.*, 2014, **79**, 11933-11939.
- 40 C. Lin, D. Y. Li, B. J. Wang, J. Z. Yao and Y. H. Zhang, *Org. Lett.*, 2015, **17**, 1328-1331.
- 41 Y. J. Liu, Y. H. Liu, S. Y. Yan and B. F. Shi, *Chem. Commun.*, 2015, **51**, 6388-6391.
- 42 Y. J. Liu, Z. Z. Zhang, S. Y. Yan, Y. H. Liu and B. F. Shi, *Chem. Commun.*, 2015, **51**, 7899-7902.

- 43 S. Maity, S. Agasti, A. M. Earsad, A. Hazra and D. Maiti, *Chem. Eur. J.*, 2015, **21**, 11320-11324.
- 44 S. Y. Yan, Y. J. Liu, B. Liu, Y. H. Liu, Z. Z. Zhang and B. F. Shi, *Chem. Commun.*, 2015, **51**, 7341-7344.
- 45 L. C. M. Castro, A. Obata, Y. Aihara and N. Chatani, *Chem. Eur. J.*, 2016, **22**, 1362-1367.
- 46 X. Yang, G. Shan, L. Wang and Y. Rao, *Tetrahedron Lett.*, 2016, **57**, 819-836.
- 47 T. Uemura, M. Yamaguchi and N. Chatani, *Angew. Chem., Int. Ed.*, 2016, **55**, 3162-3165.
- 48 V. G. Zaitsev, D. Shabashov and O. Daugulis, *J. Am. Chem. Soc.*, 2005, **127**, 13154-13155.
- 49 Z. Ruan, S. Lackner and L. Ackermann, *Angew. Chem., Int. Ed.*, 2016, **55**, 3153-3157.
- 50 H. Tang, X. R. Huang, J. N. Yao and H. Chen, *J. Org. Chem.*, 2015, **80**, 4672-4682.
- 51 H. Tang, B. W. Zhou, X. R. Huang, C. Y. Wang, J. N. Yao and H. Chen, *ACS Catal.*, 2014, **4**, 649-656.
- 52 D. Balcells, E. Clot and O. Eisenstein, *Chem. Rev.*, 2010, **110**, 749-823.
- 53 D. L. Davies, S. A. Macgregor and C. L. McMullin, *Chem. Rev.*, 2017, **117**, 8649-8709.
- 54 H. M. Omer and P. Liu, *J. Am. Chem. Soc.*, 2017, **139**, 9909-9920.
- 55 S. Singh, S. K and R. B. Sunoj, *J. Org. Chem.*, 2017, **82**, 9619-9626.
- 56 B. E. Haines, H. Y. Xu, P. Verma, X. C. Wang, J. Q. Yu and D. G. Musaev, *J. Am. Chem. Soc.*, 2015, **137**, 9022-9031.
- 57 M. D. P. Mingos, *J. Organomet. Chem.*, 2014, **751**, 153-173.
- 58 A. Y. Rogachev and R. Hoffmann, *J. Am. Chem. Soc.*, 2013, **135**, 3262-3275.
- 59 Y. Aihara and N. Chatani, *ACS Catal.*, 2016, **6**, 4323-4329.
- 60 B. Khan, R. Kant and D. Koley, *Adv. Synth. Catal.*, 2016, **358**, 2352-2358.
- 61 A. T. Higgs, P. J. Zinn and M. S. Sanford, *Organometallics*, 2010, **29**, 5446-5449.
- 62 A. T. Higgs, P. J. Zinn, S. J. Simmons and M. S. Sanford, *Organometallics*, 2009, **28**, 6142-6144.
- 63 A. L. Renz, L. M. Perez and M. B. Hall, *Organometallics*, 2011, **30**, 6365-6371.
- 64 X. C. Wang, Y. Hu, S. Bonaccorsi, Y. Hong, R. Burrell and J. Q. Yu, *J. Am. Chem. Soc.*, 2013, **135**, 10326-10329.
- 65 F. S. Han, *Chem. Soc. Rev.*, 2013, **42**, 5270-5298.
- 66 K. Wu and A. G. Doyle, *Nat. Chem.*, 2017, **9**, 779-784.
- 67 A. Amgoune and D. Bourissou, *Chem. Commun.*, 2011, **47**, 859-871.
- 68 J. Bauer, H. Braunschweig and R. D. Dewhurst, *Chem. Rev.*, 2012, **112**, 4329-4346.
- 69 L. Canovese, F. Visentin and C. Santo, *J. Organomet. Chem.*, 2014, **770**, 6-13.
- 70 A. J. Canty, M. C. Denney, B. W. Skelton and A. H. White, *Organometallics*, 2004, **23**, 1122-1131.
- 71 M. J. Zhou, T. L. Yang and L. Dang, *J. Org. Chem.*, 2016, **81**, 1006-1020.
- 72 R. E. Plata, D. E. Hall, B. E. Haines, D. G. Musaev, L. Chu, D. P. Hickey, M. S. Sigman, J. Q. Yu and D. G. Blackmond, *J. Am. Chem. Soc.*, 2017, **139**, 9238-9245.
- 73 M. Shang, S. Z. Sun, H. X. Dai and J. Q. Yu, *Org. Lett.*, 2014, **16**, 5666-5669.
- 74 M. Shang, S. Z. Sun, H. L. Wang, B. N. Laforteza, H. X. Dai and J. Q. Yu, *Angew. Chem., Int. Ed.*, 2014, **53**, 10439-10442.
- 75 M. Shang, H. L. Wang, S. Z. Sun, H. X. Dai and J. Q. Yu, *J. Am. Chem. Soc.*, 2014, **136**, 11590-11593.
- 76 S. Z. Sun, M. Shang, H. L. Wang, H. X. Lin, H. X. Dai and J. Q. Yu, *J. Org. Chem.*, 2015, **80**, 8843-8848.
- 77 H. L. Wang, M. Shang, S. Z. Sun, Z. L. Zhou, B. N. Laforteza, H. X. Dai and J. Q. Yu, *Org. Lett.*, 2015, **17**, 1228-1231.
- 78 D. Schroder, S. Shaik and H. Schwarz, *Acc. Chem. Res.*, 2000, **33**, 139-145.
- 79 M. Reinhold, J. E. McGrady and R. N. Perutz, *J. Am. Chem. Soc.*, 2004, **126**, 5268-5276.
- 80 L. S. Jongbloed, D. Garcia-Lopez, R. van Heck, M. A. Siegler, J. J. Carbo and J. I. van der Vlugt, *Inorg. Chem.*, 2016, **55**, 8041-8047.
- 81 I. P. Beletskaya and A. V. Cheprakov, *J. Organomet. Chem.*, 2004, **689**, 4055-4082.
- 82 J. Dupont, C. S. Consorti and J. Spencer, *Chem. Rev.*, 2005, **105**, 2527-2571.
- 83 A. Shiota and H. C. Malinakova, *J. Organomet. Chem.*, 2012, **704**, 9-16.
- 84 S. A. Johnson, *Dalton Trans.*, 2015, **44**, 10905-10913.
- 85 Q. Q. Lu, H. Z. Yu and Y. Fu, *J. Am. Chem. Soc.*, 2014, **136**, 8252-8260.
- 86 M. Lafrance, C. N. Rowley, T. K. Woo and K. Fagnou, *J. Am. Chem. Soc.*, 2006, **128**, 8754-8756.
- 87 B. Lian, L. Zhang, G. A. Chass and D. C. Fang, *J. Org. Chem.*, 2013, **78**, 8376-8385.
- 88 C. Mateos, J. Mendiola, M. Carpintero and J. M. Minguez, *Org. Lett.*, 2010, **12**, 4924-4927.
- 89 H. Y. Sun, S. I. Gorelsky, D. R. Stuart, L. C. Campeau and K. Fagnou, *J. Org. Chem.*, 2010, **75**, 8180-8189.
- 90 S. Rousseaux, S. I. Gorelsky, B. K. W. Chung and K. Fagnou, *J. Am. Chem. Soc.*, 2010, **132**, 10692-10705.
- 91 T. M. Figg, M. Wasa, J. Q. Yu and D. G. Musaev, *J. Am. Chem. Soc.*, 2013, **135**, 14206-14214.
- 92 H. Y. Xu, K. Muto, J. Yamaguchi, C. Y. Zhao, K. Itami and D. G. Musaev, *J. Am. Chem. Soc.*, 2014, **136**, 14834-14844.
- 93 Gaussian 09, Revision D.01, Frisch, M. J.; Trucks, G. W.; Schlegel, H. B.; Scuseria, G. E.; Robb, M. A.; Cheeseman, J. R.; Scalmani, G.; Barone, V.; Mennucci, B.; Petersson, G. A.; Nakatsuji, H.; Caricato, M.; Li, X.; Hratchian, H. P.; Izmaylov, A. F.; Bloino, J.; Zheng, G.; Sonnenberg, J. L.; Hada, M.; Ehara, M.; Toyota, K.; Fukuda, R.; Hasegawa, J.; Ishida, M.; Nakajima, T.; Honda, Y.; Kitao, O.; Nakai, H.; Vreven, T.; Montgomery, J. A., Jr.; Peralta, J. E.; Ogliaro, F.; Bearpark, M.; Heyd, J. J.; Brothers, E.; Kudin, K. N.; Staroverov, V. N.; Kobayashi, R.; Normand, J.; Raghavachari, K.; Rendell, A.; Burant, J. C.; Iyengar, S. S.; Tomasi, J.; Cossi, M.; Rega, N.; Millam, M. J.; Klene, M.; Knox, J. E.; Cross, J. B.; Bakken, V.; Adamo, C.; Jaramillo, J.; Gomperts, R.; Stratmann, R. E.; Yazyev, O.; Austin, A. J.; Cammi, R.; Pomelli, C.; Ochterski, J. W.; Martin, R. L.; Morokuma, K.; Zakrzewski, V. G.; Voth, G. A.; Salvador, P.; Dannenberg, J. J.; Dapprich, S.; Daniels, A. D.; Farkas, Ö.; Foresman, J. B.; Ortiz, J. V.; Cioslowski, J.; Fox, D. J. Gaussian, Inc., Wallingford CT, 2009.
- 94 P. J. Hay and W. R. Wadt, *J. Chem. Phys.*, 1985, **82**, 270-283.
- 95 P. J. Hay and W. R. Wadt, *J. Chem. Phys.*, 1985, **82**, 299-310.
- 96 W. R. Wadt and P. J. Hay, *J. Chem. Phys.*, 1985, **82**, 284-298.
- 97 S. Grimme, J. Antony, S. Ehrlich and H. Krieg, *J. Chem. Phys.*, 2010, **132**, 154104-154119.
- 98 E. Cancès, B. Mennucci and J. Tomasi, *J. Chem. Phys.*, 1997, **107**, 3032-3041.
- 99 B. Mennucci and J. Tomasi, *J. Chem. Phys.*, 1997, **106**, 5151-5158.

- 100 G. Scalmani and M. J. Frisch, *J. Chem. Phys.*, 2010, **132**, 114110-114124.
- 101 S. Essafi, S. Tomasi, V. K. Aggarwal and J. N. Harvey, *J. Org. Chem.*, 2014, **79**, 12148-12158.
- 102 R. E. Plata and D. A. Singleton, *J. Am. Chem. Soc.*, 2015, **137**, 3811-3826.
- 103 D. J. Marell, L. R. Furan, B. P. Woods, X. Lei, A. J. Bendel-Smith, C. J. Cramer, T. R. Hoye and K. T. Kuwata, *J. Org. Chem.*, 2015, **80**, 11744-11754.
- 104 L. F. Zou, R. S. Paton, A. Eschenmoser, T. R. Newhouse, P. S. Baran and K. N. Houk, *J. Org. Chem.*, 2013, **78**, 4037-4048.
- 105 MECPro Version 1.0.3: Minimum Energy Crossing Program (2016), Lily-Anne Hamill, Justin D. Snyder and Daniel H. Ess